

Remote Tuning of Built-In Magnetolectric Microenvironment to Promote Bone Regeneration by Modulating Cellular Exposure to Arginylglycylaspartic Acid Peptide

Wenwen Liu, Fengyi Zhang, Yuanyang Yan, Chenguang Zhang, Han Zhao, Boon Chin Heng, Ying Huang, Yang Shen, Jinxing Zhang, Lili Chen, Xiufang Wen,* and Xuliang Deng*

Mimicking the endogenous physical microenvironment is a promising strategy for biomaterial-mediated tissue regeneration. However, precise control of physical cues such as electric/magnetic fields within extracellular environments to facilitate tissue regeneration remains a formidable challenge. Here, remote tuning of the magnetolectric microenvironment is achieved by a built-in CoFe_2O_4 /poly(vinylidene fluoridetrifluoroethylene) [P(VDF-TrFE)] magnetolectric membrane for effective bone regeneration. The magnetolectric microenvironment from the nanocomposite membranes promotes osteogenic differentiation of bone marrow mesenchymal stem cells (BM-MSCs) and enhances bone defect regeneration by increasing cellular exposure and integrin binding to arginylglycylaspartic acid peptide, as predicted by molecular dynamics simulations. Moreover, BM-MSCs are directed to the osteogenic lineage by osteoimmunomodulation which involves accelerating transition from an initial inflammatory immune response to a pro-healing regenerative immune response. This work offers a strategy to mimic the magnetolectric microenvironment for achieving precise and effective tissue regenerative therapies, as well as provides fundamental insights into the biological effects driven by the built-in magnetolectric membrane, which can be remotely tuned to precisely modulate osteogenesis in situ.

1. Introduction

A major strategy in tissue engineering is to mimic the biophysical properties of target tissues and various critical aspects of the extracellular environment to modulate cell function via cell-material interactions.^[1] Recently, mimicking the endogenous physical microenvironment via implanted biomaterials has emerged as a new strategy for recapitulating the extracellular microenvironment at the wound/injury site to facilitate tissue regeneration.^[2] Endogenous magnetolectric property is an integral aspect of the natural biophysical microenvironment of native tissues,^[3] and extensive research has demonstrated that the osteogenic differentiation,^[4] chondrogenic differentiation,^[5] and neurogenic differentiation^[6] of mesenchymal stem cell (MSC) can be modulated by the application of an external electromagnetic field. The magnetolectric field provided by extracorporeal devices often

Dr. W. Liu, Dr. F. Zhang, Dr. H. Zhao, Dr. Y. Huang, Prof. X. Deng
NMPA Key Laboratory for Dental Materials National Engineering
Laboratory for Digital and Material Technology of Stomatology
Department of Geriatric Dentistry
Peking University School and Hospital of Stomatology
Beijing 100081, P. R. China
E-mail: kqdengxuliang@bjmu.edu.cn

Dr. Y. Yan, Prof. X. Wen
The School of Chemistry and Chemical Engineering
South China University of Technology Guangzhou
Guangzhou 510640, P. R. China
E-mail: xfwen@scut.edu.cn

Dr. C. Zhang
Stomatological Hospital
Southern Medical University
Guangzhou 510280, China

 The ORCID identification number(s) for the author(s) of this article can be found under <https://doi.org/10.1002/adfm.202006226>.

Prof. B. C. Heng
Central Laboratory
Peking University School and Hospital of Stomatology
Beijing 100081, P. R. China

Prof. Y. Shen
State Key Laboratory of New Ceramics and Fine Processing
Department of Materials Science and Engineering
Tsinghua University
Beijing 100084, China

Prof. J. Zhang
Department of Physics
Beijing Normal University
Beijing 100875, China

Prof. L. Chen
Department of Stomatology Union Hospital Tongji Medical College
Huazhong University of Science and Technology
Wuhan 430022, P. R. China

DOI: 10.1002/adfm.202006226

cannot work specifically and efficiently to achieve intended tissue regeneration.^[7] Moreover, accurate control of the dosage and effective working area of the external magnetoelectric stimulation is difficult to achieve.^[8] Therefore, recapitulating the natural magnetic and/or electric microenvironment at the wound/injury site by implanted biomaterials is an alternative strategy to modulate cellular and tissue biological processes for achieving optimal bone regeneration outcome, and to precisely control the in situ microenvironment for conducive tissue regeneration.^[9] Biomaterials such as magnetic nanoparticles or piezoelectric microfibers can separately provide the local magnetic or electrical field independently for tissue regeneration.^[9a] Nevertheless, this limits the synergy of electrical and magnetic stimuli, which is necessary to optimize natural cellular function.^[10]

Magnetoelectric materials exhibit a unique combination of magnetism and electric polarization, with magnetization and

electrical charge being able to be controlled simultaneously via application of a remote magnetic field,^[11] thereby effectively providing a controllable local magnetoelectric environment. Cellular behavior is known to be influenced by diurnal variations in the magnetoelectric environment, which have been studied by simulating diurnal geomagnetic variations in geomagnetic storms.^[12] Hence, to mutually couple electric and magnetic field effects and control their diurnal shifting are critical considerations for developing built-in biomaterials to mimic the in situ magnetoelectric microenvironment for the purpose of promoting tissue regeneration. Previous studies have shown that the surface potential of piezoelectric materials will typically decline by 40–50% after implantation.^[13] Through application of a remote direct current (DC) magnetic field, the magnetoelectric materials can theoretically adjust and maintain the surface potential after implantation. (Figure 1a) Beside maintaining the surface potential, the application of an external remote DC

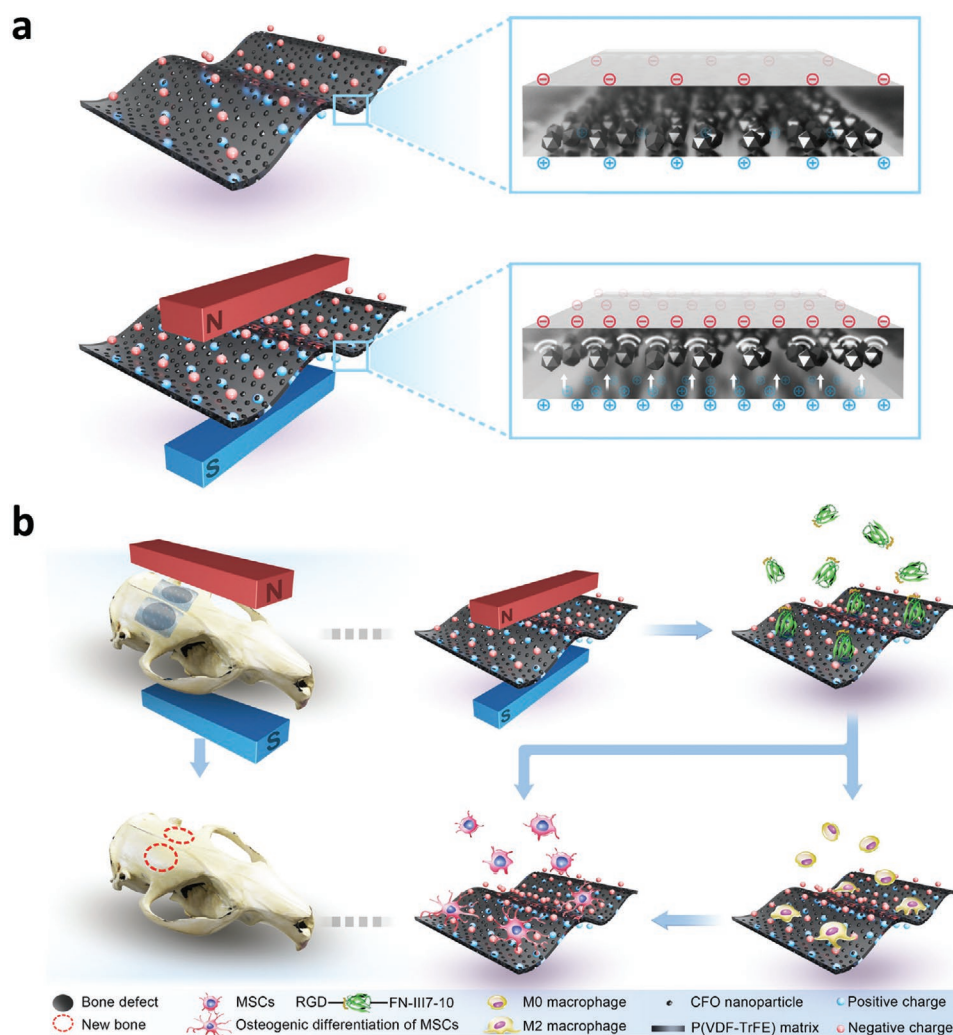


Figure 1. Illustration of magnetoelectric effects and biological effects of CFO/P(VDF-TrFE) magnetoelectric nanocomposite membranes. a) Once a magnetic field is applied to the nanocomposite membrane, strain in the magnetostrictive phase is induced, which is transmitted to the piezoelectric constituent, leading to a change in electrical polarization. b) Remote tuning of CFO/P(VDF-TrFE) magnetoelectric nanocomposite membranes via application of an external DC magnetic field promotes bone regeneration by enhancing FN adsorption, RGD exposure, macrophage polarization, and osteogenic differentiation of MSCs.

magnetic field can readily mimic the diurnal shifting magnetolectric environment.^[14] Altogether, these studies point to promising applications of magnetolectric materials in tissue regeneration.

In this study, we fabricated the CoFe₂O₄ (CFO)/poly(vinylidene fluoridetrifluoroethylene) [P(VDF-TrFE)] magnetolectric nanocomposite membranes, which can be regulated by application of a remote DC magnetic field to generate a built-in magnetolectric microenvironment. Molecular dynamics (MD) simulation was used to predict the optimal content of CFO nanoparticles for attaining the greatest arginylglycylaspartic acid (RGD) sites exposure. The magnetolectric microenvironment provided by the magnetolectric membranes can enhance osteogenesis and bone regeneration within the bone defect area. The bone regeneration can not only be attributed to the direct osteogenic effect of bone marrow mesenchymal stem cells (BM-MSCs), but also to the improved osteoimmunomodulatory microenvironment. The interaction between BM-MSCs and macrophages enhance bone repair by accelerating the transition from inflammatory immune response to regenerative immune response within the bone defect areas. (Figure 1b)

2. Results and Discussion

2.1. MD Simulation of RGD Exposure on CFO/P(VDF-TrFE) Composite Membranes

To predict the biological properties of the built-in magnetolectric microenvironment provided by our fabricated magnetolectric nanocomposite membrane, MD simulations were performed. The CFO/P(VDF-TrFE) magnetolectric nanocomposite membrane was composed of ferromagnetic CFO nanoparticles embedded within a ferroelectric P(VDF-TrFE) matrix that provide excellent flexibility for the membrane. In this study, nanocomposite membranes with 5–20 wt% CFO content were selected for the MD simulations (Figure S1a, Supporting Information). Within the simulation models (Figure S1b, Supporting Information), 10 wt% CFO content membranes exhibited the minimum distance between the FN-III7-10 protein and nanocomposite membrane (Figure S1c, Supporting Information). Additionally, the 10 wt% CFO content membranes exhibited strong interaction between the fibronectin (FN) module and the surface of the membrane, which possessed the greatest numbers of adsorbed FN-III7-10 residues within 0.35 nm (Table 1). The enhanced FN-III7-10 protein adsorption by 10 wt% CFO content membranes was also supported by the strongest van der Waals interactions and the highest value of interaction energy (Table 2). Under the influence of long-range electrostatic interactions, the protein gradually moved to the surface. As the protein gets closer to the surface, the short-range van der Waals interaction also starts to affect the protein. Therefore, the protein continuously adjusts its conformation and finally adsorbs stably on the surface, under the synergistic effects of van der Waals and electrostatic interactions. Therefore in our simulation, 10 wt% CFO content membranes were predicted to have the most favorable surface for FN-III7-10 protein adsorption.

Table 1. Number of adsorbed residues of FN-III7-10 on membranes with different CFO contents (MD simulations).

Surface	Adsorbed residues	Total
5 wt%	ASN13,ASP15,THR16,GLY17,VAL18,LEU19,GLY46,ASN47,SER48,LEU49,GLU50,GLU51,VAL52,VAL53,HIS54,ASP56,GLN57,CYS60,THR61,PHE62,ASP63,ASN64,SER66,LEU69,ASP81,ASP122,LEU123,THR124,ASN125,GLU141,SER145,PRO146,SER147,ASP148, TYR170,GLU171,GLN172,PRO289,PRO338,GLY339,ASP341, TYR366,ARG367,THR368	44
10 wt%	GLU11,ASN13,PRO14,ASP15,THR16,GLY17,VAL18,LEU19,THR20,LEU49,GLU51,VAL52,CAL53,HIS54,ALA55,ASP56,GLN57,SER59,CYS60,THR61,PHE62,ASP63,ASN64,LEU65,SER66,PRO67,ASP122, GLU141,SER145,SER147,ASP196,ILE197,GLU223,GLY249,THR250, GLU251,GLN271,SER273,THR274,VAL275,SER276,ASP277,VAL278, PRO289,GLU312,THR313,GLY314,GLY315,ASN316,SER317,LYS337, PRO338,GLY339,VAL340,ASP341, TYR366,ARG367,THR368	58
15 wt%	ASP15,GLY17,VAL18,THR32,LEU49,GLU50,GLU51,VAL52,VAL53, HIS54,ALA55,ASP56,GLN57,SER58,SER59,CYS60,THR61,PHE62, ASP63,ASN64,ASP80,GLU137,GLU141,ASP277,PRO289,GLU312, PRO338,GLY339,ASP341,ARG367,THR368	31
20 wt%	ASP56,GLN57,ASP63,ASP122,GLU137,ASP138,GLU141,SER147, GLLU171,PRO289,THR313,GLY314,ASN316,PRO338,GLY339, VAL340,ASP341,ARG367,THR368	19

RGD peptide is an archetypical ligand in the 10th type III domain of FN, which mediates cell adhesion through specific interactions with various integrin receptors.^[15] The simulation predicted that the RGD sequence on 10 wt% CFO content membranes were exposed towards the solution phase (Figure 2a), which are conducive for integrin binding. The root mean square deviation values^[16] (0.193 for 5 wt%, 0.211 for 10 wt%, 0.160 for 15 wt%, 0.148 for 20 wt%) of RGD indicated the high interdomain elasticity and flexibility of the RGD configuration in the 10 wt% CFO content membranes. The enhanced RGD elasticity and flexibility could in turn facilitate RGD-integrin binding. RGD peptide was reported to facilitate cell spreading and motility,^[17] stem cell differentiation,^[18] and nanoparticle internalization,^[17b,19] possibly through the assembly of clusters of adhesion proteins.^[20] Overall, the MD simulations indicated that the 10 wt% CFO content membranes could enhance FN-III7-10 adsorption and optimize RGD domain exposure to promote cell adhesion.^[21] According to previous studies, the FN adsorption capacity is an important extracellular environmental factor, which directly effects initial cell attachment and proliferation.^[22] Cells adhesion and spreading area was also positively correlated with increased surface RGD density.^[23] The

Table 2. The interaction energy between FN-III7-10 and membranes with different CFO contents (MD simulations).

Surface	$E_{\text{int}}^{\text{a}}$ [kJ mol ⁻¹]	$E_{\text{ele}}^{\text{b}}$ [kJ mol ⁻¹]	$E_{\text{vdw}}^{\text{c}}$ [kJ mol ⁻¹]
5 wt%	-702.725	-481.366	-221.359
10 wt%	-773.174	-431.619	-341.555
15 wt%	-701.053	-488.772	-212.281
20 wt%	-543.027	-408.092	-134.935

^{a)} E_{int} , interaction energy; ^{b)} E_{ele} , electrostatic interaction energy; ^{c)} E_{vdw} , van der Waals interaction energy.

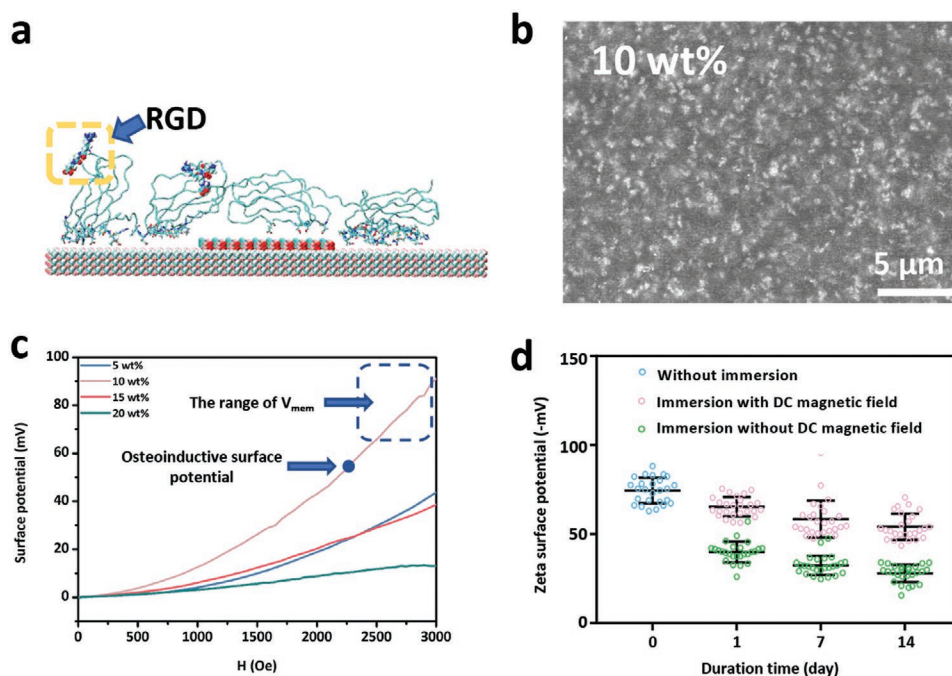


Figure 2. MD simulation and characterization of the CFO/P(VDF-TrFE) magnetolectric nanocomposite membrane a) Snapshots of the molecular dynamic simulations, showing that the RGD site was oriented towards the solution phase on the 10 wt% CFO/P(VDF-TrFE) magnetolectric membrane. b) SEM images of 10 wt% CFO/P(VDF-TrFE) membranes. c) The magnetic-field-induced surface potential of CFO/P(VDF-TrFE) membranes with different CFO content. V_{mem} : Bioelectrical communication-endogenous voltage gradients across the plasma membrane. (Typical value: -60 to -100 mV).^[48] d) Zeta potential of 10 wt% CFO/P(VDF-TrFE) membranes without immersion and membranes immersed in culture medium with or without exposure to a remote DC magnetic field after 1, 7, 14 days.

increased FN adsorption which lead to increased RGD exposure can facilitate integrin binding to enhance focal adhesion (FA) formation and effect MSC and macrophage responses to biomaterials.^[16,24] These MD simulations predict that the magnetolectric microenvironment provided by 10 wt% CFO content composite membranes could induce optimal biological effects.

2.2. Characterizing the Magnetolectric Microenvironment Provided by the CFO/P(VDF-TrFE) Nanocomposite Membranes

Based on the MD simulation, the CFO/P(VDF-TrFE) magnetolectric nanocomposite membranes with different CFO nanoparticle contents (5, 10, 15, 20 wt%) (Figure S2a, Supporting Information) were fabricated. Scanning electron microscope (SEM) imaging revealed extensive agglomeration of CFO nanoparticles at contents >15 wt% (Figure 2b; Figure S2b, Supporting Information). Homogenous dispersion of CFO nanoparticles within the piezoelectric matrix is a key prerequisite for achieving a significant magnetolectric effect.^[25] With increasing content of CFO nanoparticles, the content of the β -phase within the P(VDF-TrFE) matrix decreases, as evidenced by Fourier transform infrared spectroscopy imaging (Figure S2c, Supporting Information) and X-ray diffraction patterns (Figure S2d, Supporting Information). The β -phase is closely correlated with piezoelectric properties, as it is an electrically active phase.^[26] Consistent with the β -phase data, the piezoelectric coefficients (d_{33}) decreased with increasing

CFO nanoparticles content (Figure S2e, Supporting Information). In hysteresis loop tests, the maximum magnetization value of the different composite membranes was approximately proportional to the amount of CFO nanoparticles within the P(VDF-TrFE) matrix (Figure S2f, Supporting Information). The magnetolectric effect of the nanocomposite membranes is due to an elastic coupling interaction between electrical polarization and magnetostrictive components.^[27] Hence, appropriate CFO nanoparticle concentration within the co-polymer matrix might favor arrangement of polar conformations and therefore lead to enhanced ferroelectric and piezoelectric responses.^[28]

We next evaluated the magnetolectric effects of membranes. The magnetolectric effect, defined as the variation of the electrical polarization of a material in the presence of an applied magnetic field, or as the induced magnetization in the presence of an applied electric field, can be seen as a bridge between the electric and magnetic properties of matter.^[11] The results demonstrated that 10 wt% CFO content membranes exhibited the largest range of magnetic-field-induced surface potential (Figure 2c) among all groups after corona poling at room temperature. The magnetic-field-induced surface potential of 10 wt% CFO content membranes could be tuned from 0 to 91.15 mV by increasing the remote DC magnetic field from 0 to 3000 Oe. Our preliminary results showed that the surface potential of around 54 mV is most favorable for osteogenesis.^[26] However, the retention period of the surface potential induced by piezoelectric materials is not sufficient for optimal osteogenesis.^[13] For the magnetolectric composites, the surface

potential could be sustained for as long as required by applying a magnetic field in a non-contact manner. For instance, the nanocomposite membrane with 10 wt% of CFO content has the appropriate concentration for optimal magnetoelectric effect. The surface potential of CFO/P(VDF-TrFE) membranes were decreased after 14 days immersion in culture medium without application of a remote DC magnetic field (Figure 2d). The surface potential of 10 wt% CFO content membranes could be tuned to around 54 mV with a remote DC 23000e magnetic field, which were utilized for subsequent biological assays (Figure 2c). Upon application of a remote DC magnetic field, the surface potential of the membranes were maintained throughout 14 days of immersion in culture medium (Figure 2d). Since the diurnal geomagnetic variation has a pronounced circadian rhythmicity that exerts biological effects,^[14] a remote DC magnetic field mimicking the natural magnetic field with 12 h shifting was selected to control the magnetoelectric microenvironment in this study. The surface roughness and water contact angle measurements yielded different values according to the different nanoparticle contents of the various groups (Figure S3a,b, Supporting Information). Some researchers have reported that roughness difference, which is a microroughness level of around 100–500 nm, exert negligible effects on the cell adhesion and biological functions of larger cell types, such as BM-MSCs, osteoblasts, and neurons.^[29] The surface wettability study also showed that there is no difference in cell adhesion when the surface contact angles are around 60 to 80 degrees after 180 min of incubation.^[30] Hence, the roughness and contact angle values differences between groups should have no biological effects in this study. Tensile strength and the elastic modulus of membranes decreased along with increased CFO concentrations. However, based on our previous study, changes to the elastic modulus and tensile strength in this scale will have negligible effects on osteogenesis^[13] (Figure S3c,d, Supporting Information). Moreover, the tensile strength and elastic modulus values showed that the flexibility of the membranes could be suitable for clinical applications, such as being utilized as non-resorbable membranes to prevent the ingrowth of non-osteogenic tissues and maintain the capacity for cell occlusion.^[13,31] After corona poling, 10 wt% CFO content membranes combined with application of a remote DC magnetic field can provide an optimal controllable magnetoelectric microenvironment.

2.3. Biomimetic Magnetoelectric Microenvironment Promotes FN Adsorption and RGD Exposure That Leads to Enhanced Cell Adhesion

In biological assays, the membranes were grouped as follows: CFO 0, CFO 5, CFO 10, CFO 15, and CFO 20, which represent 0, 5, 10, 15, and 20 wt% of CFO content within membranes, respectively. E represents group with polarization treatment. M represents group exposed to a remote DC magnetic field. NC represents blank group without membrane.

To assay FN adsorption in vitro, quantitative evaluation and immunofluorescence images were used. The results demonstrated that CFO 10-E/M had the greatest FN adsorption capacity (Figure S4a–c, Supporting Information). The exposure

of the cell-binding domain of RGD on adsorbed FN was further evaluated. On CFO 10-E/M, the RGD site combined with HFN71 antibody^[32] displayed the highest intensity and biggest area among all groups (Figure S4d, Supporting Information). These results thus showed that CFO 10-E/M can enhance the FN adsorption and RGD site exposure. The enhanced FN adsorption and RGD exposure could promote cell adhesion, migration, and spreading.^[24b] Consistent with the prediction of MD simulation, the magnetoelectric microenvironment provided by CFO 10-E/M can modulate cellular behavior.

The biological performance of the CFO/P(VDF-TrFE) magnetoelectric nanocomposite membranes was further investigated. Assessment of proliferation through the cell counting kit-8 (CCK-8) assay demonstrated that there were no significant differences between groups (Figure S4e,f, Supporting Information). However, the cytoskeleton immunostaining images showed that BM-MSCs on CFO 10-E/M exhibited the largest spreading area and the most abundant FA formation among all groups (Figure S5a–f, Supporting Information). The increased FA and spreading area are correlated with enhanced RGD exposure, and might also be correlated to the osteogenic potential of BM-MSCs.^[13,33]

2.4. Biomimetic Magnetoelectric Microenvironment Enhances Osteogenesis of BM-MSCs through RGD Exposure-Mediated Cellular Mechanotransduction

The pro-osteogenic effects of the magnetoelectric microenvironment provided by CFO/P(VDF-TrFE) membranes were evaluated with BM-MSCs, under exposure to a remote DC magnetic field. The quantitative analysis of alizarin red staining demonstrated significantly higher mineralization values in CFO 10-E/M compared to membranes with different CFO contents (Figure S6a, Supporting Information). CFO 10-E/M exhibited the strongest fluorescence intensity of RUNX2 immunostaining after 3 days of incubation (Figure 3a; Figure S6d, Supporting Information). Osteogenic gene expression and protein production were further evaluated and the results showed that CFO 10-E/M upregulated the expression of osteogenesis-related genes (RUNX2, ALP, Collagen I, OCN, OSX) and proteins (OPN, BMP2, RUNX2) in the absence of osteogenic supplements (Figure 3b; Figure S6b,c,f, Supporting Information). After 7 days of culture without osteogenic supplements, higher ALP activity was detected on CFO 10-E/M (Figure S6e, Supporting Information). These results thus demonstrated that CFO 10-E/M provides an optimal magnetoelectric microenvironment for BM-MSC osteogenic differentiation.

To explore the mechanisms by which osteogenesis of BM-MSCs is promoted by enhanced FN adsorption and RGD exposure in the CFO 10-E/M group, the expression of integrin was analyzed and it was found that the gene expression and protein production levels of integrin $\alpha 5$ were significantly higher in CFO 10-E/M versus other groups (Figure 3c,d; Figure S7a, Supporting Information). Integrin $\alpha 5$ has been reported to participate in MSC osteogenesis.^[24a,34] Integrins connect the cell cytoskeleton to the microenvironment and serve as sensors of mechanical signals.^[35] Increased integrin clustering can lead to increased adhesion maturation, which in turn can modulate

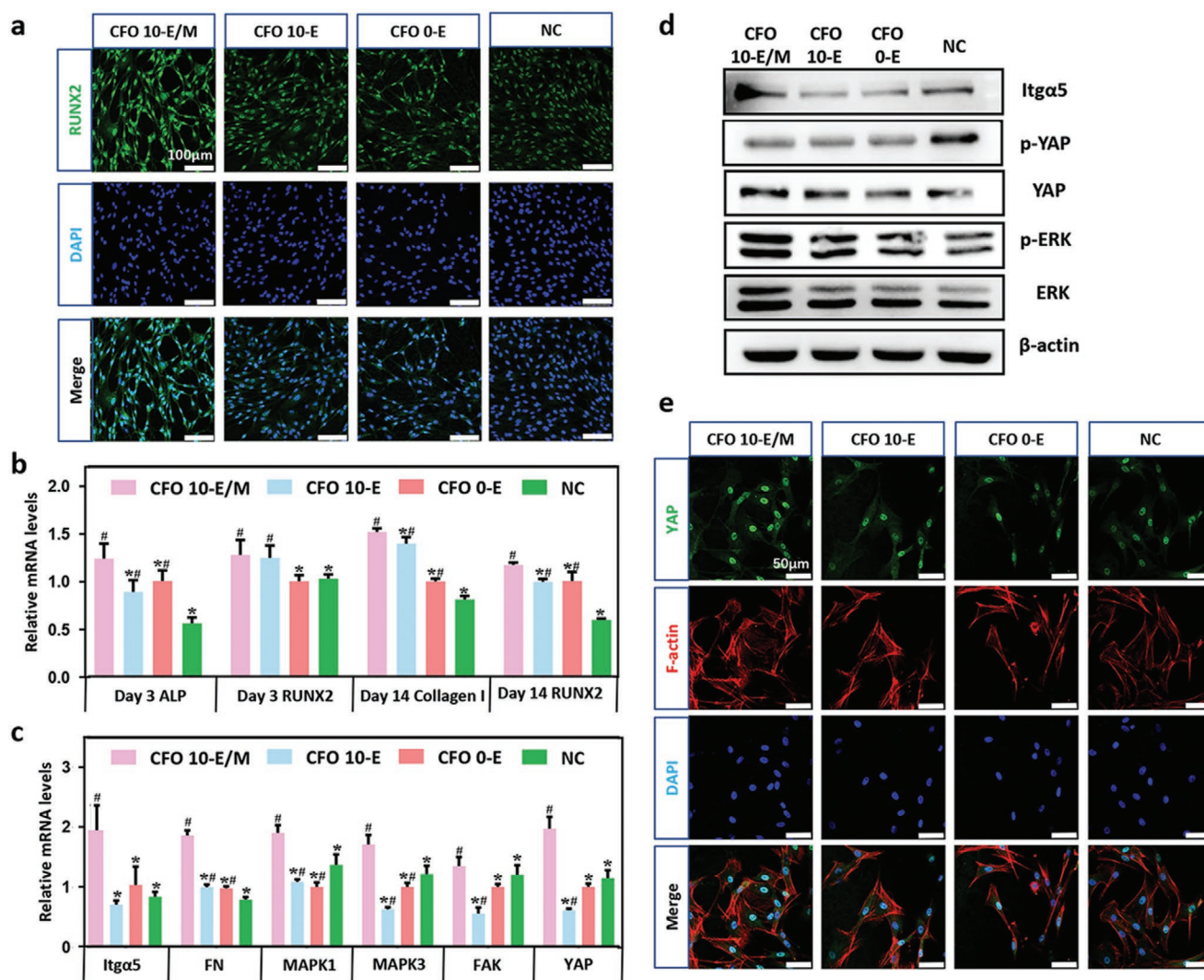


Figure 3. Osteoinductive potential of the CFO/P(VDF-TrFE) magnetolectric nanocomposite membrane and the potential mechanisms by which it induces osteogenesis in vitro. a) Immunofluorescence images showed the upregulated expression of RUNX2 in the CFO 10-E/M group (Scale bars: 100 μ m). b) RT-qPCR revealed the upregulation of osteogenic markers (ALP, RUNX2, and Collagen I) in the CFO 10-E/M group. c) RT-qPCR revealed the upregulation of Itga5, FN, MAPK1, MAPK3, FAK, and YAP in the CFO 10-E/M group. (* VS CFO 10-E/M, # VS NC, $p < 0.05$) d) Western blot analysis indicated that the CFO 10-E/M group exhibited upregulated expression of integrin α 5/ERK1/2 cascade-related proteins and increased YAP activation. e) Immunofluorescence staining showed enhanced nuclear localization of YAP in the CFO 10-E/M group (Scale bars: 50 μ m).

cell downstream signaling proteins such as ERK and nuclear localization mechanosensitive transcription regulators like YAP/TAZ.^[36] Next, we evaluated the activation of ERK signaling and YAP nuclear localization to characterize the intracellular signaling pathways. The CFO 10-E/M membrane markedly upregulated the gene expression levels of ERK1/2, which were consistent with increased protein expression (Figure 3c,d). Immunofluorescence staining showed that YAP is concentrated within the cell nuclei on CFO 10-E/M (Figure 3e). The statistical analysis of fluorescence intensity ratios between the cell's nucleus and cytoplasm demonstrated that nuclear localization of YAP is significantly higher on CFO 10-E/M versus the other membrane groups (Figure S7b, Supporting Information). The protein expression results showed that BM-MSCs cultured on CFO 10-E/M displayed increased YAP but decreased

phosphorylated-YAP (Figure 3d), which were consistent with the immunostaining results. Therefore, we propose that the magnetolectric microenvironment provided by CFO 10-E/M induces BM-MSC osteogenic differentiation by increasing RGD exposure and initiating sensors of biomechanical signaling, which in turn promotes FA maturation and trigger a series of mechanotransduction-related molecular processes, involving the activation of ERK signaling and nuclear localization of YAP.

2.5. Biomimetic Magnetolectric Microenvironment Modulates Osteoimmunomodulatory Responses In Vitro

Bone regeneration is a highly complex process which involves various different cell types such as immune cells, progenitor

cells, and MSC.^[37] Macrophages are the first cell type to arrive at the bone defect site, and have long been thought to contribute to the initial inflammation and debridement of the injury location.^[38] Mounting evidence has shown that macrophage polarization is a key regulator of bone regeneration.^[39]

To further investigate the osteoimmunomodulatory effects of the magnetoelectric microenvironment, we evaluated the polarization of macrophages and osteogenic differentiation of BM-MSCs within a co-culture system. Macrophages were seeded on the nanocomposite membranes, while BM-MSC were seeded in the upper chambers of transwell culture dishes. Macrophages cultured on CFO 10-E/M expressed high expression levels of CD206, which is the M2 marker (Figure 4a,b; Figures S8a and S13a, Supporting Information). Meanwhile, there is no significant change in the expression of the M1 marker CCR7 (Figure S8b,c, Supporting Information) by macrophages cultured on CFO 10-E/M, as compared with the other groups. The results proved that CFO 10-E/M could promote M2 polarization of macrophages. The immunofluorescence staining showed that expression levels of integrin $\alpha 5$, integrin $\beta 1$, and vinculin in macrophages were increased (Figures S9–S11,

Supporting Information). These elevated integrin expression levels on CFO 10-E/M indicated that the magnetoelectric microenvironment could enhance macrophage polarization through integrin-related pathways. The western blot results showed that the protein expression levels of integrin $\beta 1$, phosphorylation levels of phosphoinositide 3-kinase (PI3K) and serine/threonine kinase Akt (Akt) were increased in the CFO 10-E/M group (Figure S12a, Supporting Information). The CFO 10-E/M group exhibited the strongest fluorescence intensity of phosphorylated Akt immunostaining (Figure S12b, Supporting Information). Furthermore, the western blot results showed that the CFO 10-E/M group had significantly reduced nuclear factor kappa B (NF- κ B/p65) levels compared to other groups (Figure S12a, Supporting Information). Protein adsorption and integrin binding interactions have been demonstrated to modulate inflammation.^[24c,32,40] On CFO 10-E/M, the enhanced FN adsorption resulted in adoption of an active conformation that led to more RGD binding site exposure and increased macrophage integrin $\beta 1$ binding. Increased integrin $\beta 1$ binding activates PI3K/Akt signaling, leading to the inhibition of NF- κ B activation and subsequent anti-inflammatory polarization (M2)

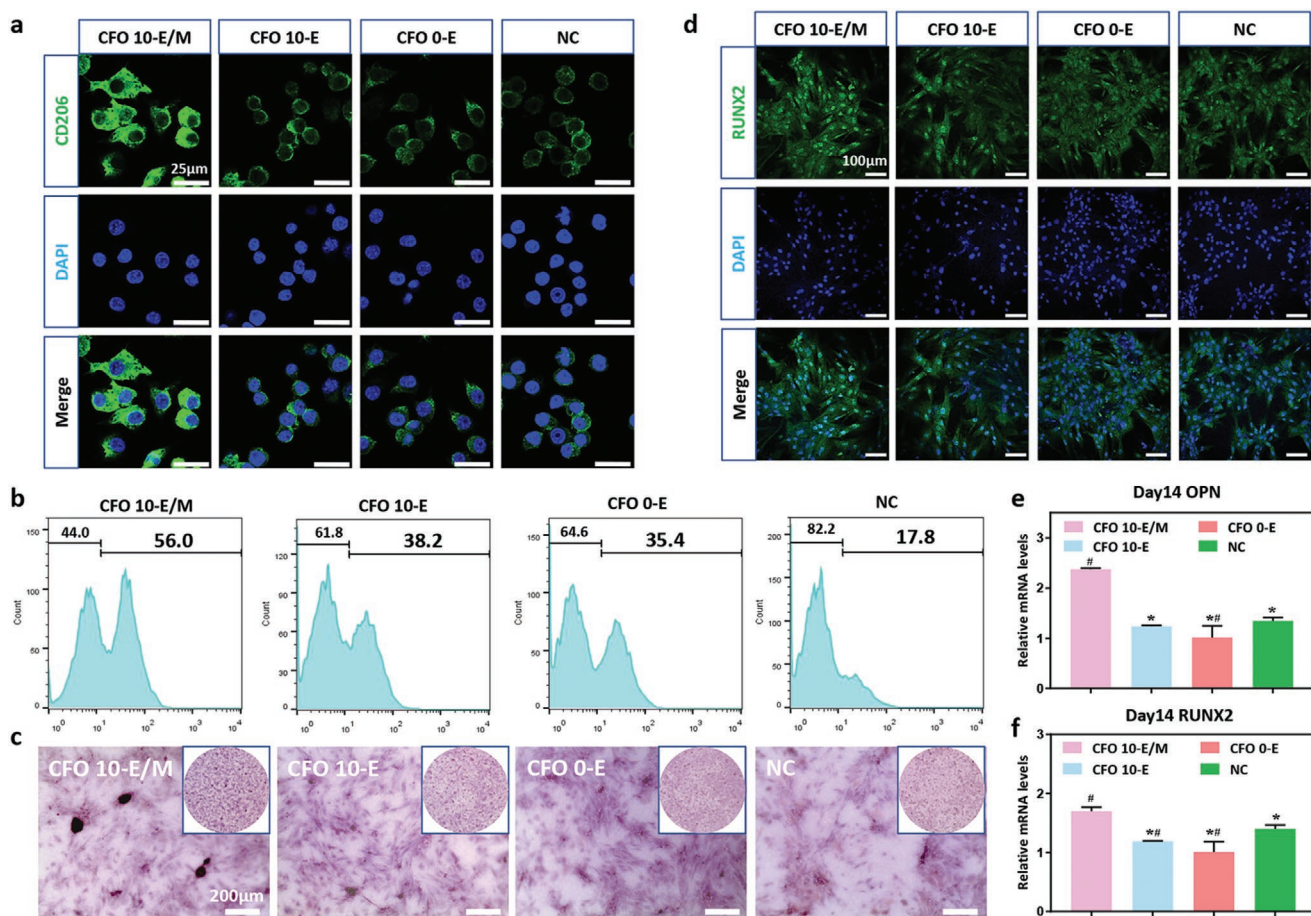


Figure 4. Macrophage polarization and osteogenesis of BM-MSC on CFO/P(VDF-TrFE) magnetoelectric nanocomposite membranes in vitro. a) Immunostaining images and b) FC analysis of CD206 expression, which indicated that the CFO 10-E/M group promoted macrophage M2 polarization in the co-culture system (Scale bars: 25 μ m). c) Alizarin red staining (Scale bars: 200 μ m), d) immunostaining images of RUNX2 expression (scale bars: 100 μ m) and e,f) RT-qPCR analysis showing that the CFO 10-E/M group enhanced BM-MSC osteogenesis in the co-culture system. (* VS CFO 10-E/M, # VS NC, $p < 0.05$).

of macrophages.^[32] Hence, our data indicated that the RGD-integrin binding induced PI3K/Akt activation could be one of the potential mechanisms by which the CFO10-E/M group mediates M2 polarization of macrophages.

To evaluate osteogenic differentiation in this co-culture system, ALP activity (Figure S13b, Supporting Information), alizarin red staining (Figure 4c), immunofluorescence staining (Figure 4d), and osteogenic gene expression (Figure 4e,f) analysis were performed. CFO 10-E/M exhibited the most BM-MSCs osteogenic differentiation among all groups. Macrophages with M2 phenotype secrete cytokines, such as IL-10, BMP2, and VEGF, which in turn modulate mesenchymal progenitor cell recruitment, angiogenesis and bone regeneration.^[41] Therefore, M2 polarization of macrophages is one important mechanism by which BM-MSCs osteogenic differentiation is promoted by the magnetoelectric microenvironment.

2.6. Biomimetic Magnetoelectric Microenvironment Accelerates Bone Regeneration In Vivo

The therapeutic efficacy of the magnetoelectric nanocomposite membranes on bone defect repair were further investigated in vivo. The magnetoelectric nanocomposite membranes were implanted to cover critical-sized (5 mm) calvarial defects in mature rats.^[26] The P(VDF-TrFE) based membrane was not sticky to the newly regenerated bone tissue,^[13] which facilitates subsequent removal of the membrane and bone defect healing without residual materials. Since the removable membrane can be remotely tuned with an external DC magnetic field, the removed membranes have the potential to be reusable. Histological analysis of Masson's trichrome staining and H&E staining showed that the CFO 10-E/M led to complete healing, with flat and consecutive bone structures in 8 weeks. The mature osteoid tissue was present in the top center region of the defect in the CFO 10-E/M group. These results revealed that the CFO 10-E/M membrane promoted more new bone formation than the other groups (Figure S14a,b, Supporting Information). In micro-CT tests, the CFO 10-E/M group demonstrated the most new bone formation at all-time points. After 4 and 8 weeks post-surgery, the CFO 10-E/M group demonstrated homogeneous and contiguous regenerated mature bone tissue within the defect area. By contrast, in the other groups, new bone tissue formed mostly at the marginal areas around the original bone defect (Figure 5a; Figure S14c, Supporting Information). Quantitative analysis revealed that the CFO 10-E/M membrane significantly increased regenerated bone volume after 8 weeks of implantation (Figure 5b). These results thus confirmed that the magnetoelectric microenvironment provided by the CFO 10-E/M membrane promotes enhanced bone regeneration in vivo.

2.7. Biomimetic Magnetoelectric Microenvironment Modulates Osteoimmunomodulatory Responses In Vivo

The osteoimmunomodulatory effects of the built-in magnetoelectric microenvironment were further investigated in vivo. After 1 day of implantation, adherent macrophages on the CFO

10-E/M membrane exhibited the strongest immunostaining intensity of CCR7 (Figure S15, Supporting Information) amongst all groups. The immunostaining signals of CD206 were weak in all groups (Figure S17, Supporting Information). After 4 days of implantation, cells from the interstitial fluid collected at the defect region of the CFO 10-E/M group showed the highest ratio of CD11c-positive cells (M1 macrophage marker) among all groups (Figure S18a, Supporting Information). M1 macrophages contribute to an initial acute inflammatory stage in vivo.^[38] Meanwhile, the protein spectrum results demonstrated that complement components such as C1r, Cfh, C5, Cfb, and C8b were upregulated in the CFO 10-E/M group. Enrichment of immune-related pathways and biological processes, such as endocytosis, complement, and coagulation cascade were also detected in the CFO 10-E/M group (Figure 5c,d; Figure S16b, Supporting Information). There is increasing evidence that the complement system, a crucial arm of the innate immune system, plays an important role in bone homeostasis, regeneration, and inflammation.^[42a] The activated coagulation and complement products can recruit immune cells to the injury site, which leads to a simultaneous early inflammatory response.^[42] Bone regeneration can be modulated by these inflammatory molecules.^[43] M1 phenotype macrophages arrived at the injury site during the initial stage and are involved in the early inflammatory response.^[44] In this study, the early M1 macrophage response in vivo could not be detected by in vitro testing, and this might be because the complex osteoimmunomodulatory environment of the bone defect area is difficult to mimic in vitro.^[37b] These results thus imply that the CFO 10-E/M membrane could trigger the initial immune response during the early stage of bone repair.

We next evaluated the process of M1 to M2 transition affected by built-in magnetoelectric microenvironment in vivo. After 4 days of implantation, assessment of adherent macrophages on the nanocomposite membranes showed that the immunostaining intensity of CD206 in the CFO 10-E/M group was stronger than the other groups (Figure 5e) and that the immunostaining intensity of CCR7 in the CFO 10-E/M group was weaker than the other groups (Figure S15, Supporting Information). After 14 days of implantation, adherent macrophages on the nanocomposite membrane and cells from the interstitial fluid collected at the defect regions of the CFO 10-E/M group exhibited the highest ratio of M2 macrophages. (Figures S17 and S18b, Supporting Information) Meanwhile, the adherent macrophages on nanocomposite membranes demonstrated the weakest CCR7 immunostaining signals in the CFO 10-E/M group (Figure S16a, Supporting Information). Notably, macrophage M2 polarization happened earlier on the membrane than in the interstitial fluid of the CFO 10-E/M group, which suggested that the cells adherent on the membrane can sense the magnetoelectric microenvironment directly and further accelerate the transition from the M1 to M2 phenotype. Cells within the membrane proximity will sense the magnetoelectric microenvironment later than cells that are in direct contact with the membrane. Since bone is a highly dynamic organ, the fracture healing is affected by the surrounding fracture microenvironment, such as inflammatory processes.^[45] The interstitial fluid provides the 3D environment for inflammatory response, which is important for

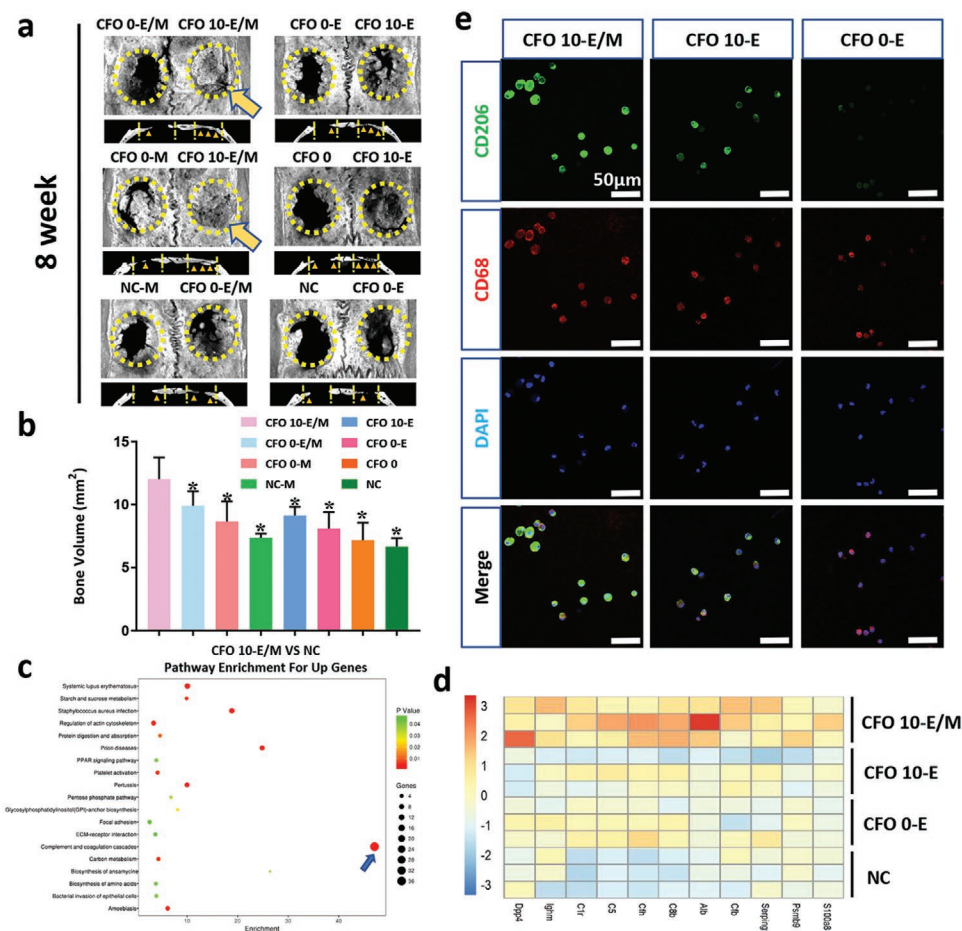


Figure 5. CFO/P(VDF-TrFE) magnetolectric nanocomposite membrane mediated bone regeneration and immune response in vivo. a) Representative CT images of bone regeneration within rat cranial defects at 8 weeks after membrane implantation, with the CFO 10-E/M group exhibiting the most abundant new bone formation. Yellow arrows indicate enhanced bone regeneration in the CFO 10-E/M group. Yellow triangles denote new bone. Yellow dotted lines denote the boundary between nascent bone and host bone. b) Quantitative analysis of the total volume of newly formed bone tissue. (* VS CFO 10-E/M, $p < 0.05$) c) KEGG pathway analysis, d) heat map demonstrating that some immune-related proteins and pathways were upregulated in the CFO 10-E/M group. Blue arrow indicates the enriched genes in the complement and coagulation cascades pathway of the CFO 10-E/M group. e) Immunofluorescence images of CD206 expression, indicating that the CFO 10-E/M membrane promoted adherent macrophage M2 polarization (Scale bars: 50 μm).

bone regeneration. After initial inflammation, the phenotype was transitioned to M2 at the remodeling stage. M2 macrophages are known as the pro-healing phenotype.^[46] Many biomaterials have been designed to promote tissue regeneration by activating M2 polarization of macrophages.^[47] Taken together, these results thus indicated that the CFO 10-E/M membranes could activate the initial immune response and accelerate the transition from M1 to M2 phenotype to further promote bone regeneration. Therefore, our findings suggested that the CFO 10-E/M membrane could provide a magnetolectric microenvironment with 12h remote DC magnetic field shifting to enhance bone regeneration by activating the immune response and accelerating the transition from the acute inflammation stage to bone healing stage.

The remotely tuned magnetolectric microenvironment provided by the removable and easily shaping membrane have the potential to be utilized clinically for space maintenance and bone regeneration.

3. Conclusion

This study developed a flexible and reusable magnetolectric nanocomposite membrane for bone regeneration which can be regulated by a remote DC magnetic field to mimic the natural magnetolectric microenvironment. Based on MD simulations together with biological evaluation, the 10 wt% CFO/P(VDF-TrFE) magnetolectric nanocomposite membranes were confirmed to be the optimal group for promoting bone regeneration by increasing RGD exposure. Moreover, the magnetolectric microenvironment provided by the magnetolectric nanocomposite membrane not only directly enhanced BM-MS-C osteogenic differentiation, but also regulated the osteoimmunomodulatory environment to improve bone regeneration. The osteoimmunomodulatory microenvironment within the bone defect area triggered initial inflammation and then subsequently promoted M1 to M2 transition of macrophages. Our research thus provides a novel strategy of remote tuning

of the magnetoelectric microenvironment for precisely controlling bone regeneration in situ, which holds much promise for achieving efficient bone repair in the clinic.

4. Experimental Section

Details of the materials and experimental methods used are available in the Supporting Information.

Supporting Information

Supporting Information is available from the Wiley Online Library or from the author.

Acknowledgements

W.L. and F.Z. contributed equally to this work. This work was supported by the National Key R&D Program of China (2018YFC1105303/04, 2018YFE0194400), National Natural Science Foundation of China (81600905, 81991505, 31670993), Peking University Medicine Fund of Fostering Young Scholars' Scientific & Technological Innovation supported by the Fundamental Research Funds for the Central Universities (BMU2018PY005), Beijing Municipal Natural Science Foundation (7182185), and Key Science and Technology Program of Hunan Province (2017WK2041). All animal experiments were conducted with the approval of the Animal Care and Use Committee of Peking University (IACUC number: LA2019161).

Conflict of Interest

The authors declare no conflict of interest.

Keywords

arginylglycylaspartic acid, bone regeneration, magnetoelectric microenvironments, nanocomposite membranes, remote tuning

Received: July 23, 2020

Revised: September 15, 2020

Published online:

- [1] S. W. Benoit, P. S. Danielle, A. R. D. Michael, K. S. Anseth, *Nat. Mater.* **2008**, *7*, 816.
- [2] a) W. Li, Z. Yan, J. Ren, X. Qu, *Chem. Soc. Rev.* **2018**, *47*, 8639; b) G. Thrivikraman, G. Madras, B. Basu, *Biomaterials* **2016**, *77*, 26.
- [3] A. Maziarz, B. Kocan, M. Bester, S. Budzik, M. Cholewa, T. Ochiya, A. Banas, *Stem Cell Res. Ther.* **2016**, *7*, 54.
- [4] a) P. Fomby, A. J. Cherlin, A. Hadjizadeh, C. J. Doillon, V. Sueblinvong, D. J. Weiss, J. H. T. Bates, T. Gilbert, W. C. Liles, C. Lutzko, J. Rajagopal, D. J. Prockop, D. Chambers, A. Giangreco, A. Keating, D. Kotton, P. I. Lelkes, D. E. Wagner, D. J. Prockop, *Ann. Am. Thorac. Soc.* **2010**, *12*, 181; b) J. Chen, C. Tu, X. Tang, H. Li, J. Yan, Y. Ma, H. Wu, C. Liu, *Stem Cell Res. Ther.* **2019**, *10*, 1.
- [5] C. Tu, Y. Xiao, Y. Ma, H. Wu, M. Song, *Stem Cell Res. Ther.* **2018**, *9*, 215.
- [6] a) Y. Seong, J. Moon, J. Kim, *Life Sci.* **2014**, *102*, 16; b) H. J. Kim, J. Jung, J. H. Park, J. H. Kim, K. N. Ko, C. W. Kim, *Exp. Biol. Med.* **2013**, *238*, 923.
- [7] J. J. Cook, N. J. Summers, E. A. Cook, *Clin. Podiatr. Med. Surg.* **2015**, *32*, 45.
- [8] C. Daish, R. Blanchard, K. Fox, P. Pivonka, E. Pirogova, *Ann. Biomed. Eng.* **2018**, *46*, 525.
- [9] a) H. M. Yun, S. J. Ahn, K. R. Park, M. J. Kim, J. J. Kim, G. Z. Jin, H. W. Kim, E. C. Kim, *Biomaterials* **2016**, *85*, 88; b) S. M. Dadfar, K. Roemhild, N. I. Drude, S. von Stillfried, R. Knüchel, F. Kiessling, T. Lammers, *Adv. Drug Delivery Rev.* **2019**, *138*, 302; c) C. Ning, Z. Zhou, G. Tan, Y. Zhu, C. Mao, *Prog. Polym. Sci.* **2018**, *81*, 144.
- [10] M. Cifra, J. Z. Fields, A. Farhadi, *Prog. Biophys. Mol. Biol.* **2011**, *105*, 223.
- [11] P. Martins, S. Lanceros-Méndez, *Adv. Funct. Mater.* **2013**, *23*, 3371.
- [12] a) V. V. Krylov, E. A. Osipova, N. A. Pankova, M. G. Talikina, Y. V. Chebotareva, Y. G. Izumov, A. A. Batrakova, V. A. Nepomnyashchikh, *Biofizika* **2017**, *62*, 675; b) V. V. Krylov, N. P. Kantserova, L. A. Lysenko, E. A. Osipova, *Int. J. Biometeorol.* **2019**, *63*, 241.
- [13] X. Zhang, C. Zhang, Y. Lin, P. Hu, Y. Shen, K. Wang, S. Meng, Y. Chai, X. Dai, X. Liu, Y. Liu, X. Mo, C. Cao, S. Li, X. Deng, L. Chen, *ACS Nano* **2016**, *10*, 7279.
- [14] V. V. Krylov, *Bioelectromagnetics* **2017**, *38*, 497.
- [15] a) M. D. Pierschbacher, E. Ruoslahti, *Nature* **1984**, *309*, 30; b) E. Ruoslahti, *Annu. Rev. Cell Dev. Biol.* **1996**, *12*, 697.
- [16] Y. Wei, S. Jiang, M. Si, X. Zhang, J. Liu, Z. Wang, C. Cao, J. Huang, H. Huang, L. Chen, S. Wang, C. Feng, X. Deng, L. Jiang, *Adv. Mater.* **2019**, *31*, 1900582.
- [17] a) M. Schvartzman, M. Palma, J. Sable, J. Abramson, X. Hu, M. P. Sheetz, S. J. Wind, *Nano Lett.* **2011**, *11*, 1306; b) J. Lam, T. Segura, *Biomaterials* **2013**, *34*, 3938.
- [18] T. Re'em, O. Tsur-Gang, S. Cohen, *Biomaterials* **2010**, *31*, 6746.
- [19] H. J. Kong, S. Hsiong, D. J. Mooney, *Nano Lett.* **2007**, *7*, 161.
- [20] a) H. Shroff, C. G. Galbraith, J. A. Galbraith, H. White, J. Gillette, S. Olenych, M. W. Davidson, E. Betzig, *Proc. Natl. Acad. Sci. U. S. A.* **2007**, *104*, 20308; b) R. Changede, H. Cai, S. J. Wind, M. P. Sheetz, *Nat. Mater.* **2019**, *18*, 1366.
- [21] a) X. Ren, Y. Feng, J. Guo, H. Wang, Q. Li, J. Yang, X. Hao, J. Lv, N. Ma, W. Li, *Chem. Soc. Rev.* **2015**, *44*, 5680; b) E. Ruoslahti, M. Pierschbacher, *Science* **1987**, *238*, 491.
- [22] a) S. J. Chae, J. U. Lee, G. H. Kim, *Colloids Surf., B* **2019**, *181*, 408; b) H. T. Aiyelabegan, E. Sadroddiny, *Biomed. Pharmacother.* **2017**, *88*, 956.
- [23] G. Koçer, P. Jonkheijm, *Adv. Healthcare Mater.* **2017**, *6*, 1600862.
- [24] a) Z. Hamidouche, O. Fromigué, J. Ringe, T. Häupl, P. Vaudin, J. C. Pagès, S. Srouji, E. Livne, P. J. Marie, *Proc. Natl. Acad. Sci. U. S. A.* **2009**, *106*, 18587; b) P. Chatakun, R. Núñez-Toldrà, E. J. Díaz López, C. Gil-Recio, E. Martínez-Sarrà, F. Hernández-Alfaro, E. Ferrés-Padró, L. Giner-Tarrida, M. Atari, *Cell. Mol. Life Sci.* **2014**, *71*, 113; c) T. D. Zaveri, J. S. Lewis, N. V. Dolgova, M. J. Clare-Salzler, B. G. Keselowsky, *Biomaterials* **2014**, *35*, 3504.
- [25] P. Martins, R. Gonçalves, S. Lanceros-Mendez, A. Lasheras, J. Gutiérrez, J. M. Barandiarán, *Appl. Surf. Sci.* **2014**, *313*, 215.
- [26] C. Zhang, W. Liu, C. Cao, F. Zhang, Q. Tang, S. Ma, J. J. Zhao, L. Hu, Y. Shen, L. Chen, *Adv. Healthcare Mater.* **2018**, *7*, 1701466.
- [27] a) Y. Zong, Z. Yue, P. Martins, J. Zhuang, Y. Du, S. Lanceros-Mendez, M. J. Higgins, *Nanoscale* **2018**, *10*, 17370; b) B. Tang, J. Zhuang, L. Wang, B. Zhang, S. Lin, F. Jia, L. Dong, Q. Wang, K. Cheng, W. Weng, *ACS Appl. Mater. Interfaces* **2018**, *10*, 7841.
- [28] P. Martins, A. Lasheras, J. Gutierrez, J. M. Barandiaran, I. Orue, S. Lanceros-Mendez, *J. Phys. D: Appl. Phys.* **2011**, *44*, 495303.
- [29] a) H.-I. Chang, Y. Wang, in *Regenerative Medicine and Tissue Engineering - Cells and Biomaterials*, (Ed: D. Eberli), InTech, London **2011**, pp. 993–1001; b) J. M. Rice, J. A. Hunt, J. A. Gallagher, P. Hanarp, D. S. Sutherland, J. Gold, *Biomaterials* **2003**, *24*, 4799; c) J. Yang, Y. Zhou, F. Wei, Y. Xiao, *Clin. Oral Impl. Res.* **2016**, *27*, 1031.
- [30] a) J. Wei, T. Igarashi, N. Okumori, T. Igarashi, T. Maetani, B. Liu, M. Yoshinari, *Biomed. Mater.* **2009**, *4*, 045002; b) G. Perumal,

- P. M. Sivakumar, A. M. Nandkumar, M. Doble, *Mater. Sci. Eng., C* **2020**, *109*, 110527.
- [31] a) R. Dimitriou, G. I. Mataliotakis, G. M. Calori, P. V. Giannoudis, *BMC Med.* **2012**, *10*, 81; b) C. Dahlin, A. Linde, J. Gottlow, S. Nyman, *Plast. Reconstr. Surg.* **1988**, *81*, 672.
- [32] L. Lv, Y. Xie, K. Li, T. Hu, X. Lu, Y. Cao, X. Zheng, *Adv. Healthcare Mater.* **2018**, *7*, 1800675.
- [33] a) R. McBeath, D. M. Pirone, C. M. Nelson, K. Bhadriraju, C. S. Chen, *Dev. Cell* **2004**, *6*, 483; b) X. Yao, R. Peng, J. Ding, *Adv. Mater.* **2013**, *25*, 5257; c) W. Liu, Y. Wei, X. Zhang, M. Xu, X. Yang, X. Deng, *ACS Nano* **2013**, *7*, 6928; d) B. Wang, Q. Cai, S. Zhang, X. Yang, X. Deng, *J. Mech. Behav. Biomed. Mater.* **2011**, *4*, 600.
- [34] P. J. Marie, *Nat. Rev. Endocrinol.* **2013**, *9*, 288.
- [35] J. Z. Kechagia, J. Ivaska, P. Roca-Cusachs, *Nat. Rev. Mol. Cell Biol.* **2019**, *20*, 457.
- [36] a) A. M. Pasapera, I. C. Schneider, E. Rericha, D. D. Schlaepfer, C. M. Waterman, *J. Cell Biol.* **2010**, *188*, 877; b) M. J. Paszek, N. Zahir, K. R. Johnson, J. N. Lakin, G. I. Rozenberg, A. Gefen, C. A. Reinhart-King, S. S. Margulies, M. Dembo, D. Boettiger, D. A. Hammer, V. M. Weaver, *Cancer Cell* **2005**, *8*, 241; c) L. Chang, L. Azzolin, D. Di Biagio, F. Zanconato, G. Battilana, R. Lucon Xiccato, M. Aragona, S. Giulitti, T. Panciera, A. Gandin, G. Sigismondo, J. Krijgsveld, M. Fassan, G. Brusatin, M. Cordenonsi, S. Piccolo, *Nature* **2018**, *563*, 265; d) A. Elosegui-Artola, I. Andreu, A. E. M. Beedle, A. Lezamiz, M. Uroz, A. J. Kosmalska, R. Oria, J. Z. Kechagia, P. Rico-Lastres, A. L. Le Roux, C. M. Shanahan, X. Trepas, D. Navajas, S. Garcia-Manyes, P. Roca-Cusachs, *Cell* **2017**, *171*, 1397; e) H. Wolfenson, B. Yang, M. P. Sheetz, *Annu. Rev. Physiol.* **2019**, *81*, 585; f) H. Cao, W. Zhang, F. Meng, J. Guo, D. Wang, S. Qian, X. Jiang, X. Liu, P. K. Chu, *ACS Appl. Mater. Interfaces* **2017**, *9*, 5149; g) H. W. Park, Y. C. Kim, B. Yu, T. Moroishi, J. S. Mo, S. W. Plouffe, Z. Meng, K. C. Lin, F. X. Yu, C. M. Alexander, C. Y. Wang, K. L. Guan, *Cell* **2015**, *162*, 780; h) P. Han, J. E. Frith, G. A. Gomez, A. S. Yap, G. M. O'Neill, J. J. Cooper-White, *ACS Nano* **2019**, *13*, 11129; i) C. Loebel, R. L. Mauck, J. A. Burdick, *Nat. Mater.* **2019**, *18*, 883.
- [37] a) K. Schmidt-Bleek, A. Petersen, A. Dienelt, C. Schwarz, G. N. Duda, *Expert Opin. Biol. Ther.* **2014**, *14*, 247; b) C. Schlundt, H. Schell, S. B. Goodman, G. Vunjak-Novakovic, G. N. Duda, K. Schmidt-Bleek, *J. Exp. Orthop.* **2015**, *2*, 1.
- [38] J. Pajarinen, T. Lin, E. Gibon, Y. Kohno, M. Maruyama, K. Nathan, L. Lu, Z. Yao, S. B. Goodman, *Biomaterials* **2019**, *196*, 80.
- [39] a) C. Yin, Q. Zhao, W. Li, Z. Zhao, J. Wang, T. Deng, P. Zhang, K. Shen, Z. Li, Y. Zhang, *Acta Biomater.* **2020**, *102*, 416; b) W. Liu, J. Li, M. Cheng, Q. Wang, K. W. K. Yeung, P. K. Chu, X. Zhang, *Adv. Sci.* **2018**, *5*, 1800749.
- [40] I. G. Luzina, N. W. Todd, N. Nacu, V. Locketell, J. Choi, L. K. Hummers, S. P. Atamas, *Arthritis Rheum.* **2009**, *60*, 1530.
- [41] a) L. J. Raggatt, M. E. Wulschleger, K. A. Alexander, A. C. K. Wu, S. M. Millard, S. Kaur, M. L. Maughan, L. S. Gregory, R. Steck, A. R. Pettit, *Am. J. Pathol.* **2014**, *184*, 3192; b) P. Qiu, M. Li, K. Chen, B. Fang, P. Chen, Z. Tang, X. Lin, S. Fan, *Biomaterials* **2020**, *227*, 119552.
- [42] a) Y. Mödinger, G. Q. Teixeira, C. Neidlinger-Wilke, A. Ignatius, *Int. J. Mol. Sci.* **2018**, *19*, 3367; b) M. Huber-Lang, A. Kovtun, A. Ignatius, *Semin. Immunol.* **2013**, *25*, 73.
- [43] Y. Zhu, P. Jiang, B. Luo, F. Lan, J. He, Y. Wu, *Nanoscale* **2019**, *11*, 6817.
- [44] M. L. Novak, T. J. Koh, *J. Leukocyte Biol.* **2013**, *93*, 875.
- [45] L. Claes, S. Recknagel, A. Ignatius, *Nat. Rev. Rheumatol.* **2012**, *8*, 133.
- [46] a) H. Kang, H. J. Jung, S. K. Kim, D. S. H. Wong, S. Lin, G. Li, V. P. Dravid, L. Bian, *ACS Nano* **2018**, *12*, 5978; b) P. J. Murray, J. E. Allen, S. K. Biswas, E. A. Fisher, D. W. Gilroy, S. Goerd, S. Gordon, J. A. Hamilton, L. B. Ivashkiv, T. Lawrence, M. Locati, A. Mantovani, F. O. Martinez, J. L. Mege, D. M. Mosser, G. Natoli, J. P. Saeij, J. L. Schultze, K. A. Shirey, A. Sica, J. Suttles, I. Udalova, J. A. vanGinderachter, S. N. Vogel, T. A. Wynn, *Immunity* **2014**, *41*, 14.
- [47] a) J. Han, Y. S. Kim, M. Y. Lim, H. Y. Kim, S. Kong, M. Kang, Y. W. Choo, J. H. Jun, S. Ryu, H. Y. Jeong, J. Park, G. J. Jeong, J. C. Lee, G. H. Eom, Y. Ahn, B. S. Kim, *ACS Nano* **2018**, *12*, 1959; b) K. L. Spiller, S. Nassiri, C. E. Witherel, R. R. Anfang, J. Ng, K. R. Nakazawa, T. Yu, G. Vunjak-Novakovic, *Biomaterials* **2015**, *37*, 194.
- [48] C. Ribeiro, V. Sencadas, D. M. Correia, S. Lanceros-Méndez, *Colloids Surf., B* **2015**, *136*, 46.